# A simulation of skin mitochondrial PO2 in circulatory shock

Hilderink, Bashar N; Crane, Reinier F; Baysan, Meryem; Arbous, Sesmu; van den Bogaard, Bas; Mik, Egbert G; Ince, Can; Pillay, Janesh; Juffermans, Nicole P

*Published in:*
Journal of Applied Physiology

*DOI:*
10.1152/japplphysiol.00621.2022



*Publication date:*
2023

american physiological society
JOURNAL OF APPLIED PHYSIOLOGY

J Appl Physiol 134: 1165–1176, 2023.
First published March 17, 2023; doi:10.1152/japplphysiol.00621.2022

RESEARCH ARTICLE

# A simulation of skin mitochondrial $Po_2$ in circulatory shock

**Bashar N. Hilderink,[1] Reinier F. Crane,[1] Meryem Baysan,[2] Sesmu M. Arbous,[2] Bas van den Bogaard,[1] Egbert G. Mik,[3] Can Ince,[4] Janesh Pillay,[5] and Nicole P. Juffermans[1,4]**

*[1]Department of Intensive Care, OLVG Hospital, Amsterdam, The Netherlands; [2]Department of Intensive Care, LUMC, Leiden, The Netherlands; [3]Laboratory of Experimental Anesthesiology, Department of Anesthesiology, Erasmus Medical Center, Rotterdam, The Netherlands; [4]Laboratory of Translational Intensive Care, Erasmus MC, University Medical Center, Rotterdam, The Netherlands; and [5]Department of Critical Care, University Medical Center Groningen, University of Groningen, Groningen, The Netherlands*

## Abstract

Circulatory shock is the inadequacy to supply mitochondria with enough oxygen to sustain aerobic energy metabolism. A novel noninvasive bedside measurement was recently introduced to monitor the mitochondrial oxygen tension in the skin (mito$Po_2$). As the most downstream marker of oxygen balance in the skin, mito$Po_2$ may provide additional information to improve shock management. However, a physiological basis for the interpretation of mito$Po_2$ values has not been established yet. In this paper, we developed a mathematical model of skin mito$Po_2$ using a network of parallel microvessels, based on Krogh's cylinder model. The model contains skin blood flow velocity, heterogeneity of blood flow, hematocrit, arteriolar oxygen saturation, and mitochondrial oxygen consumption as major variables. The major results of the model show that normal physiological mito$Po_2$ is in the range of 40–60 mmHg. The relationship of mito$Po_2$ with skin blood flow velocity follows a logarithmic growth curve, reaching a plateau at high skin blood flow velocity, suggesting that oxygen balance remains stable while peripheral perfusion declines. The model shows that a critical range exists where mito$Po_2$ rapidly deteriorates if skin perfusion further decreases. The model intuitively shows how tissue hypoxia could occur in the setting of septic shock, due to the profound impact of microcirculatory disturbance on mito$Po_2$, even at sustained cardiac output. Mito$Po_2$ is the result of a complex interaction between all factors of oxygen delivery and microcirculation. This mathematical framework can be used to interpret mito$Po_2$ values in shock, with the potential to enhance personalized clinical trial design.

**NEW & NOTEWORTHY** This is the first paper to simulate mitochondrial oxygen tension in skin in circulatory shock. The relationships of mito$Po_2$ with parameters of (microcirculatory) oxygen delivery aid in the understanding of noninvasive bedside measurement of mito$Po_2$ values and show that mitochondrial oxygen tension is two orders of magnitude higher than classically assumed. The model can be used to enhance clinical trial design investigating mito$Po_2$ as a resuscitation target in circulatory shock.

*mathematical model; mitochondrial oxygen tension; mito$Po_2$; oxygen; shock*

## INTRODUCTION

Circulatory shock is considered as the inadequacy of the cardiovascular system to supply enough oxygen to maintain aerobic cellular respiration. Ensuring adequate tissue oxygenation of the vital organs in the presence of critical illness is the central dogma of intensive care medicine. Historically, the cornerstone of resuscitation has conventionally been to restore macro hemodynamic parameters (such as mean arterial pressure and cardiac output) to normal levels, presuming that this would improve cellular oxygen availability. However, it is widely established that restoration of macro hemodynamic variables in shock often is dissociated from an improvement in cellular oxygen deficit, and consequently, from patient outcome (1). Thereby, the focus of shock management has shifted toward surrogate markers of microcirculation and oxygen supply and demand balance. Lactate, capillary refill time (CRT), sublingual dark-field imaging (SDF), and near-infrared spectroscopy (NIRS) are used as a proxy of cellular oxygen deficit in shock and as triggers to guide interventions. However, these are indirect markers, contributing to the risk of over- or under-resuscitation, both of which are associated with adverse outcomes (2).

Theoretically, the most downstream marker of oxygen supply and demand balance would be at the level of the mitochondria in the vital organs (3). The recent development of the protoporphyrin-IX delayed fluorescence lifetime technique (PpIX-TSLT) allows for real-time noninvasive assessment of mitochondrial oxygen tension (mito$Po_2$) in skin. This technique requires saturation of the heme synthesis pathway by applying a skin patch containing 5-aminolevulinic acid (ALA) (4, 5). In multiple animal experimental models and human pilot studies, this technique was able to indicate

Correspondence: B. N. Hilderink (b.n.hilderink@olvg.nl).
Submitted 20 October 2022 / Revised 7 March 2023 / Accepted 8 March 2023

impaired mitochondrial oxygen availability at the organ level, even before deterioration of other markers of tissue hypoxia, such as an increase in lactate (6–8). As skin mito$P_{O_2}$ is also easily accessible for measurement, it may be a promising marker of shock and potentially an ideal endpoint of resuscitation.

However, because of the novelty of this technique, a physiological interpretation of mito$P_{O_2}$ is lacking. Such a foundational framework is required to interpret mito$P_{O_2}$ values in the eventual monitoring and treatment of circulatory shock. It would otherwise remain unclear which mito$P_{O_2}$ values indicate adequate tissue oxygenation and which values indicate a deficit in oxygen delivery and thus a potential trigger for resuscitative interventions.

The majority of models focus on brain or skeletal muscle tissue oxygenation (9–13). Mathematical models of skin tissue oxygenation have remained lacking due to the absence of interest in the oxygen supply to the skin in critical care and exercise physiology. Skin mito$P_{O_2}$ is thought to reflect total body oxygen debt and is presumed to reflect the microcirculation (6, 14). However, many questions remain regarding its interpretation. How does mito$P_{O_2}$ respond to changes in skin perfusion? To what extent do other parameters of oxygen delivery and the microcirculation affect mito$P_{O_2}$ and how does the dependency of mito$P_{O_2}$ on skin perfusion change when these variables are changed? And importantly, can mito$P_{O_2}$ indicate tissue hypoxia in the setting of hyperdynamic shock?

In this paper, we developed a mathematical model of mitochondrial oxygen tension to understand the behavior of skin mito$P_{O_2}$ in the context of circulatory shock using a network of parallel microvessels, based on Krogh's cylinder model.

## METHODS

### Study Procedures

We model skin mito$P_{O_2}$ in the context of circulatory shock. As mito$P_{O_2}$ is only clinically measurable on skin, we use the term mito$P_{O_2}$ to refer to skin mitochondrial oxygen tension. We simulate mito$P_{O_2}$ as a function of the most often altered parameters in shock: skin perfusion (skin blood flow velocity), hematocrit, arterial oxygen saturation (arteriolar), oxygen utilization/consumption, and microcirculatory dysfunction (flow heterogeneity, decrease in microvessel density, and diffusion impairment). Mito$P_{O_2}$ is modeled as a function of skin microcirculatory parameters. However, many microcirculatory parameters differ in definition and values from their systemic counterparts, i.e., systemic versus microcirculatory hematocrit. As such, to enhance clinical interpretation of our model, the microcirculatory parameters and constants are derived from the systemic values.

First, we simulate mito$P_{O_2}$ as a function of skin blood flow velocity, with all other parameters held constant. Next, we expand by varying additional variables to investigate how this relationship is shifted when oxygen saturation, hematocrit, and oxygen consumption change. To account for microcirculatory disturbances in our model, we first analyze the sensitivity of mito$P_{O_2}$ to variation in capillary density, heterogeneity, and diffusivity and simulate the effect of the most commonly found microcirculatory disturbances in shock.

Second, we investigate how shock alters mito$P_{O_2}$ by modeling simultaneous changes in peripheral perfusion, microcirculatory heterogeneity, and oxygen saturation.

We use the Krogh cylinder model as the basis of our model and expand it to account for an array of these cylinders, to reflect a network of microvessels in the skin. The most significant assumptions of our modified Krogh model are *1*) no discrete arteriolar wall resistance to diffusion, *2*) tissue $O_2$ consumption is uniform, *3*) all microvessels are parallel, unbranched, and equally spaced, and *4*) capillaries and first-order arterioles (diameter 10 μm) are the only microvessels that play a role in $O_2$ transport. More complex models of unequal-spaced networks have been developed to circumvent these assumptions and to account for arteriovenous and intercapillary oxygen diffusion (9). These models approximate experimental data of critical extraction ratios in muscle better. However, analytical studies have shown that the simplifications of the Krogh model mostly impact predictions of $O_2$ extraction at the capillary edge but not the center (15). No experimental data are available on the arteriolar wall resistance to oxygen diffusion but modeling studies have shown that it is close or equal to that of the surrounding tissue as first-order arterioles are composed of endothelium and a layer of smooth muscle cells (16, 17). Therefore, these assumptions will have only minor effect on the average tissue oxygen tension.

MATLAB (Mathworks Inc, Natick, MA) is used to computationally solve the equations with the parameters and constants shown in Table 1 and to produce the graphs.

### Clinical Validation of the Model

We validate our model findings by fitting a selection data of yet unpublished data from another clinical study of 44 patients after cardiac surgery. All study procedures were performed in accordance with the relevant guidelines and regulations.

Lactate levels of these patients were recorded bihourly concurrently with mito$P_{O_2}$ measurements. We fit the lactate level as measure of anaerobic metabolism to the predicted relation of mito$P_{O_2}$ with skin oxygen extraction ratio (OER) which is the ratio of oxygen consumed ($\dot{V}O_2$) to oxygen supply ($DO_2$) and is calculated using the relationship $OER = SaO_2 - SvmicO_2/SaO_2$ where $SvmicO_2$ is the outflow oxygen saturation at the end of the microvessel. As such, mito$P_{O_2}$ is related to a well-understood and, at a systemic level, clinically measurable parameter of oxygen delivery. The critical skin OER, at which anaerobic metabolism occurs, is assumed 0.6 (35), equal to the global systemic critical OER, as no experimentally determined value of OER specific to the skin is available. The clinical data are fitted to a model with baseline parameters and varying SkBV.

### The Mathematical Model

We model mito$P_{O_2}$ using the Krogh cylinder model of a single microvessel, see Fig. 1 (arteriolar and capillary). Mito$P_{O_2}$ is the average tissue $P_{O_2}$ around all the microvessels in the area of interest. The tissue $P_{O_2}$ around a single microvessel is the volume-averaged triple integral of the $P_{O_2}$ at every point [$P_{O_{2tissue}}(r,z)$] around this cylinder, where $r$ is the radial distance and $z$ is the longitudinal distance (see Fig. 1).

**Table 1.** *Parameter and constant values used in model*

| Parameter | Value |
|---|---|
| Tissue cylinder radius, $R_t$ | 60 μm (18, 19) |
| Microvessel radius, $R_c$ | 10 μm (20) |
| Microvessel hematocrit, H | 0.31 (21–23) |
| Inflow Hb saturation into microvessel, $SaO_2$ | 92% (24–26) |
| Skin oxygen consumption, m | 0.2 to 0.5 × $10^{-4}$ $mLO_2/mL/s$ (27) |
| Baseline value of skin blood flow velocity, v | 0.05 cm/s (28) |
| Skin blood flow heterogeneity, σ | 0.01 to 0.09 (29) |
| Krogh coefficient of tissue, $K_t$ | 1 × $10^{-9}$ (30) |
| Krogh coefficient of extracellular fluid, $K_e$ | 8.3 × $10^{-10}$ (31) |
| Volume fraction of extracellular space φ | 0.2 (32, 33) |

This is expressed mathematically as:

$$tissuePO_2\ around\ single\ microvessel = \frac{1}{Volume}\int_0^{2\pi}\int_0^{L}\int_0^{R_t} PO_{2tissue}(r,z,\theta)\,dr\,dz\,d\theta \quad (1)$$

To obtain the mitoPo$_2$, tissuePo$_2$ of all the microvessels is averaged:

$$mitoPO_2 = \frac{\sum tissuePO_2\ single\ microvessel}{number\ of\ microvessels} \quad (2)$$

The Po$_2$ of the tissue cylinder around a single microvessel can be found using the Krogh-Erlang equation, which computes the Po$_2$ at every point around a microvessel from the capillary oxygen tension at a certain distance $z$ and radial distance $r$ from the entrance of the capillary [$P_{cap}(z)$]. At each incremental distance, oxygen is "lost" to the tissue depending on the oxygen consumption (m), the oxygen diffusivity ($D$), the solubility coefficient of oxygen in tissue (α), the radius of the tissue cylinder in cm ($R_t$), and the radius of the capillary in cm ($R_c$) (9, 10, 36–39):

$$P_{tissue}(r,z) = P_{cap}(z) - \frac{m}{D\alpha}\left(\frac{R_t^2}{2}\ln\frac{r}{R_c}\right) + \frac{m}{4D\alpha}\left(r^2 - R_c^2\right) \quad (3)$$

This gives rise to estimation of the tissue oxygen tension. To estimate the intramitochondrial oxygen tension, resistance of the tissue that is supplied by the cells must be computed. This resistance to diffusion is greater due to the higher concentration of protein contained in cells. The resistance to diffusion by cells requires a different computation of the Krogh constant. The following formula (*Eq. 4*) to calculate the separate Krogh diffusivities was developed and validated previously (40–42):

$$K_t = \varphi K_e + (1-\varphi)K_c \quad (4)$$

$K_t$ is the tissue Krogh constant, $K_e$ is the Krogh constant of the extracellular fluid, and $K_c$ is the Krogh constant of the cells. The Krogh constant is the product of diffusivity (D) and solubility (α). φ is the proportion of volume that is extracellular fluid. From experimentally determined values for $K_e$, $K_t$, and the volume fraction of extracellular space of the epidermis/dermis, the diffusivity, $K_c$ of cells in a parallel arrangement can be calculated. $K_c$ is then substituted in *Eq. 3* to yield the oxygen tension inside the cells around the microvessel. The classically held belief that the Po$_2$ drops as much as 30 mmHg across the mitochondrial membrane in the oxygen cascade has been experimentally and theoretically demonstrated to be false in accordance with fundamental diffusion theory (36, 43, 44). The Po$_2$ drop across the mitochondrial membrane is only few hundredths of mmHg at normal oxygen consumption in the absence of mitochondrial clustering around capillaries (45, 46). There is no evidence of mitochondrial clustering in skin and therefore the mitochondrial Po$_2$ is equal to the intracellular $O_2$ tension calculated with *Eqs. 3* and *4*.

The decrease in $P_{cap}(z)$ when blood moves along the vessel as compared with entrance of the capillary can be described according to a mass-balance equation for oxygen (9, 12, 36):

$$SO_2(z) = SaO_2 - \frac{m\left(R_t^2 - R_c^2\right)}{H{*}Chb{*}v} \times z \quad (5)$$

where H is capillary discharge hematocrit, Chb is oxygen binding capacity of Hb and v is individual skin blood flow velocity. The partial pressure of oxygen [Pcap($z$)] is computed from oxygen saturation [So$_2$($z$)] by the inverse Hill equation governing the Hb-$O_2$ dissociation curve, which can be substituted back into *Eq. 3*:

$$P_{cap}(z) = p_{50}\left(\frac{SO_2(z)}{1-SO_2(z)}\right)^{\frac{1}{n}} \quad (6)$$

The above model describes the mitoPo$_2$ assuming a network comprising identical microvessels, with equal blood flow velocities (v). To expand the model to account for variation in heterogeneity of microvessel flow as seen in sepsis, we will use a probability density function. This probability density function denotes the proportion or frequency of microvessels that have a certain blood flow velocity while the average skin blood flow velocity remains constant. This is frequently modeled using a gamma distribution (denoted as H), which returns the proportion of microvessels that

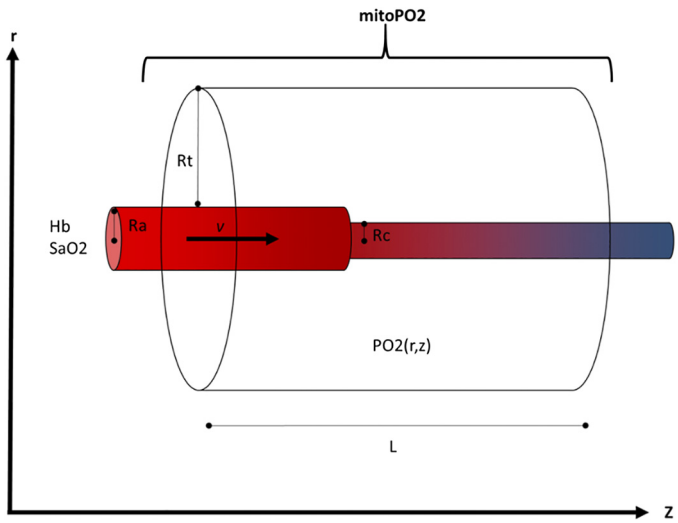


**Figure 1.** Schematic of Krogh cylinder of microvessel unit composed of arteriole and capillary. $SaO_2$, entrance Hb $O_2$ saturation at arteriolar inlet. Po$_2$(r,z) is the Po$_2$ at any point along the $z$ and $r$ axes in the tissue cylinder. L, length of microvessel and tissue cylinder. MitoPo$_2$ is the average of the integral of Po$_2$(r,z) with boundaries of tissue cylinder. MitoPo$_2$, mitochondrial oxygen tension in the skin; Hb, hemoglobin; Ra, radius of arteriole; Rc, radius of capillary, Rt, radius of tissue cylinder; v, skin blood flow velocity.

have a certain individual blood flow velocity (μ), ranging from 0 (no microvessels have this velocity) to 1 (all microvessels have that velocity) (13, 47, 48). This proportion is dependent on the shape of the gamma distribution which varies with standard deviation of the blood flow velocities (σ) and the average skin blood flow velocity of all microvessels together (ν).

MitoPo$_2$ of single microvessels with individual velocities [MitoPo$_2$(μ)] are then computed and computationally integrated to yield the mean mitoPo$_2$ over a network as following:

$$mitoPO_2(v) = \int_0^\infty d\mu\, miPO_2(\mu) \cdot H(\sigma, v, \mu) \tag{7}$$

To check the correctness of the set of equations (*Eqs. 1–6*), we have performed dimensional analysis.

The equations are dimensionally homogenous since:
Pcap and mitoPo$_2$ have dimensions of M L$^{-1}$ T$^{-2}$
M has dimensions of T$^{-1}$
Z has dimensions of L
V has dimensions of L T$^{-1}$
Chb has dimensions of M$^{-1}$
K has dimensions of M$^{-1}$ L3 T
Z has dimensions L
R$_c$ and R have dimensions L
So$_2$ is dimensionless

Furthermore, we define dimensionless parameter $\varepsilon = \frac{R_t}{r_c}$, which denotes the ratio of the tissue cylinder to the capillary radius. From the dimensional analysis using Rayleigh's method, we identified dimensionless parameter $\rho = K * \frac{\varepsilon}{m * R_t}$, which can be interpreted as the absorption of oxygen into the tissue cylinder around the capillary. Henceforth the governing equations become: $\Delta SO_2(z) = \frac{m(\varepsilon-1)}{H*Chb*v} * z$, which itself is dimensionless and represents the extraction ratio of oxygen in the tissue cylinder, and $P_{tissue}(r,z) = P_{cap}(z) - \frac{1}{2\rho r_c}\left(\ln\frac{r}{R_c}\right) + \frac{\varepsilon}{\rho}\left(r^2 - R_c^2\right)$, which is the Krogh equation expressed in terms of dimensionless parameters ρ and ε.

## Choice of Values for Constants and Parameters Used in the Model

*Tissue cylinder radius ($R_t$).* The skin has distinct microcirculatory geometry, with variations in capillary density in different regions of the skin and thus modeling of mitoPo$_2$ in skin must take into account the area and depth of the fluorescence signal originating from protoporphyrin IX, induced by an aminolevulinic acid (5-ALA) containing patch. Although often assumed that 5-ALA is localized exclusively to the epidermis, in vivo evidence indicates that substantial amounts of fluorescence signal originate from the upper layers of the dermis (49). The microvessel network supplying the upper dermis and epidermis originates from a superficial plexus of horizontal arterioles in the subcutaneous tissue. The microvessel loops, consisting of first-order arterioles and capillaries, have a total length of 1,000–3,000 μm (50, 51). We model the microvessel loops with the assumption that countercurrent exchange of $O_2$ does not occur between the arterial and venous end. Previous modeling works have shown that countercurrent exchange of oxygen is negligible in skin capillary loops and that the oxygen tension around it is primarily determined by the longitudinal gradients (30).

From histopathological findings of cadaver thoracic skin, the interloop distance is found to range between 110 and 140 μm, depending on the site of skin (18, 19). A mean cylinder radius of 60 μm will be used in the model (120 μm/2 capillaries). To model loss of capillary density on mitoPo$_2$, the $R_t$ will be varied.

*Microvessel radius ($R_c$).* The radius of skin capillaries is 4–5 μm, and of first-order arterioles is 15 μm (20). Because the upper dermis is also supplied by first-order arterioles, these must also be taken into account in the microvessel radius. To approximate the combined radius of a capillary and first-order arteriole, we will assume that half the microvessel is a capillary and half is first-order arteriole, the average radius of the complete microvessel segment is therefore 10 μm.

*Skin blood flow velocity (v).* Mean values for skin blood flow velocity (SkBV) have been reported to be between 0.4 and 0.6 cm/s with a total range observed from 0.1 cm/s to 0.9 cm/s in nonheated skin with a mean temperature of 32–34°C (28). In patients with shock, the average decrease in SkBV, as measured with laser doppler, ranges from 60% to 95% when compared with healthy human volunteers (52). For our shock simulation, we will use a conservative decrease in SkBV of 60% which equates to 0.02 cm/s.

*Skin oxygen consumption (m).* Studies have used different methods and experimental setups to quantify skin oxygen consumption. An oxygen consumption rate in skin (m) of 0.33 × 10$^{-4}$ mL $O_2$/mL/s with range of 0.25–0.45 × 10$^{-4}$ mL $O_2$/mL/s was previously determined using transcutaneous oxygen electrodes heated to 37°C (27). This value for *m* in skin corresponds approximately to half of total body oxygen consumption (volume averaged) and one-third of resting muscle tissue oxygen consumption (20).

*Inflow Hb saturation into microvessel ($SaO_2$).* Controversy exists on the inlet Hb saturation into capillaries (9). Experimental data in muscle show that 30–40% of oxygen loss to surrounding tissue occurs before the capillary segment ($SaO_2$ of 60–70%) (24, 25). However, other data suggest that the observations are due to overestimation of convective $O_2$ transport at up and downstream points (17, 53, 54). Because our microvessel segment consists of arteriole and capillary, the entrance saturation is set at 92%, as only a small amount of desaturation occurs before first-order arterioles (26).

*Microvessel hematocrit (H).* Due to the ratio between the red blood cells and capillary radius, microvessel hematocrit can be defined in two ways: discharge hematocrit and tube hematocrit. Discharge hematocrit is defined as the proportion of RBCs exiting a microvessel and is experimentally found to be 22% less than systemic hematocrit, independent of blood velocity (21–23). In contrast, the tube hematocrit is the volume proportion of RBCs inside a capillary at any snapshot in time and varies substantially with blood flow velocity and vessel diameter and can be as low as 5% (21–23). Our model uses the discharge hematocrit, as we are only concerned with the rate of the RBCs as oxygen-carrying packets flowing through the capillary (9, 36) and not the proportion of RBCs over the whole length of the microvessel. Assuming a systemic hematocrit of 0.4, the microvessel hematocrit is 0.31.

*Capillary flow heterogeneity ($\sigma$).* Experimental and computational studies have shown that in shock states, the blood flow throughout a network is highly heterogenous and can be approximated using a gamma distribution (55). Common values found for the standard deviation of the distribution of blood flow inside capillaries range from 0 to 0.1 cm/s, depending on the pathology (56). On average, patients with septic shock show a 10-fold increase in the standard deviation of SkBV distribution in the sublingual microcirculation compared with healthy volunteers (29). It is unknown whether this is an accurate representation of the situation in the skin. Nevertheless, to approximate the interplay between heterogeneity of SkBV, during shock, we will vary the heterogeneity from 0.01 to 0.09. For the normal physiological state, we will assume a heterogeneity of 0. Figure 2 shows an example of the gamma distributions showing the frequencies of blood flow velocities in the microvessel network.

## RESULTS

### Variation of mitoPo$_2$ with Skin Blood Flow Velocity, Hematocrit, and Oxygen Saturation

We present the results of mitoPo$_2$ in terms of parameters of oxygen delivery. At a baseline SkBV of 0.05 cm/s (physiological situation), the mitoPo$_2$ was 48 ± 8 mmHg (Fig. 3). Maximum mitoPo$_2$ slightly increased to 53 ± 7 mmHg at supraphysiological SkBV. The relationship between mitoPo$_2$ and SkBV approximates a logarithmic growth curve. When SkBV decreased to 0.03 cm/s, the curve remained a plateau and hence mitoPo$_2$ remains stable. Upon further decrease in SkBV to 0.02 cm/s, the mitoPo$_2$ curve showed a steep decline, and hence, below this value, small changes in SkBV lead to large decrements in mitoPo$_2$.

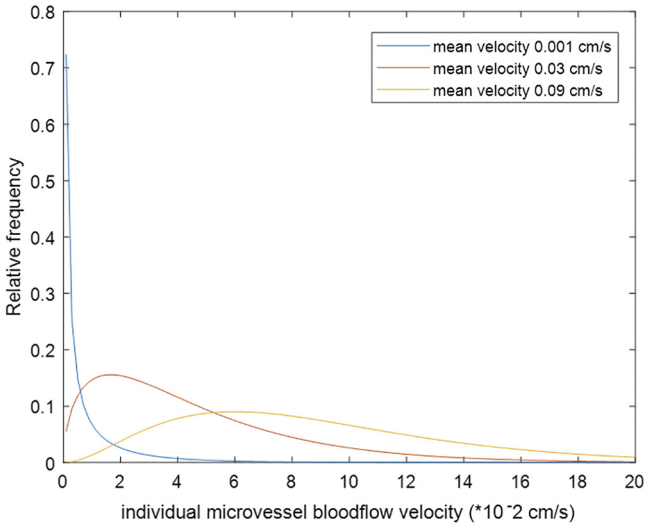


**Figure 2.** Frequency plots of gamma distributions used to model flow heterogeneity. Blue line shows the distribution of individual microvessel velocities when the mean skin blood flow velocity of complete network is 0.001 cm/s and standard deviation is 0.03 cm/s. Orange line shows the distribution of individual microvessel velocities when the mean of complete network is 0.03 cm/s and standard deviation is 0.03 cm/s. Yellow line shows the distribution of individual microvessel velocities when the mean of complete network is 0.09 cm/s and standard deviation is 0.03 cm/s.

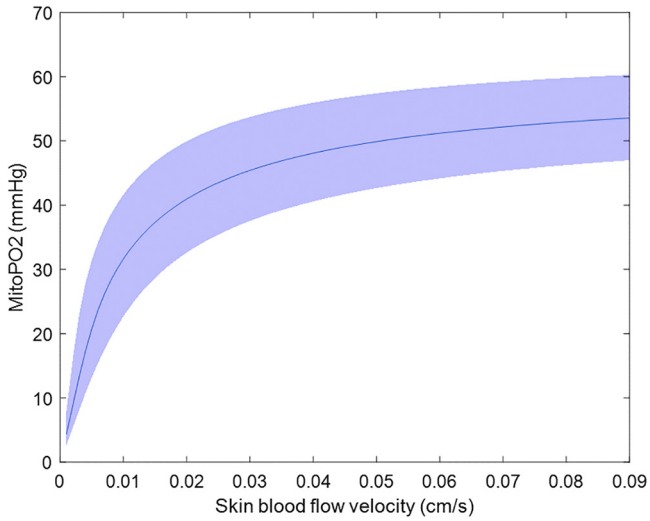


**Figure 3.** Graph showing relationship between MitoPo$_2$ and skin blood flow velocity. The shaded area indicates the range of oxygen consumption between 0.2 and 0.5 $\times$ $10^{-4}$ mL/O$_2$/mL/s. The blue line represents an oxygen consumption of 0.35 $\times$ $10^{-4}$ mL/O$_2$/mL/s. MitoPo$_2$, mitochondrial oxygen tension in the skin.

The change in mitoPo$_2$ in relation to Hb-O$_2$ saturation and hematocrit is shown in Fig. 4, *A* and *B,* respectively. It can be seen that the effect of SaO$_2$ was negligible at low SkBV, until SkBV rises to 0.01 cm/s. However, at low oxygen saturations, the plateau was reached at a lower SkBV. Furthermore, the mitoPo$_2$-SkBV plateau exponentially increased with increases in oxygen saturation, with a step from 83% to 86% only increasing mitoPo$_2$ from 30 to 35 mmHg, whereas the step from 92% to 95% increased mitoPo$_2$ from 50 mmHg to 65 mmHg.

The variation of the mitoPo$_2$-SkBV curve with hematocrit followed a logarithmic relationship, further increases in hematocrit will lead to smaller increases in mitoPo$_2$. From a baseline microvessel hematocrit of 31%, a drop in hematocrit did not affect mitoPo$_2$ until a hematocrit of 14%, and this effect is seen throughout the whole range of SkBV.

### Effect of Microcirculatory Disturbances on mitoPo$_2$

Figure 5 shows the effects of flow heterogeneity, capillary density, and diffusion resistance on the mitoPo$_2$-SkBV curve. Heterogeneity of SkBV had the largest impact. A standard deviation of 0.09 in the distribution of vessels resulted in a decrease of 30 mmHg in mitoPo$_2$ at SkBV of 0.05 cm/s when compared with homogenous flow (5 A). In addition, with heterogeneous flow, mitoPo$_2$ could not reach values above 38 mmHg, even at maximal SkBV.

Loss of 50% of the microvessel density (the intervessel distance, represented by the ratio of radius of the tissue cylinder to the capillary radius, $\varepsilon$), resulted in a decrease in mitoPo$_2$ of 10–20 mmHg in the intermediate range of SkBV (0.03–0.06 cm/s). The effect of capillary density on mitoPo$_2$ was approximately linear, as evidenced by the equispacing of the curves in Fig. 5*B*. Loss of vessel density rendered the relation between mitoPo$_2$ and SkBV slightly more linear. Diffusivity (4 C) had almost no effect on mitoPo$_2$. Diffusivity was modeled as a proxy of resistance to oxygen diffusion and can decrease substantially in edematous states. A 50% decrease in D of the tissue surrounding the microvessels

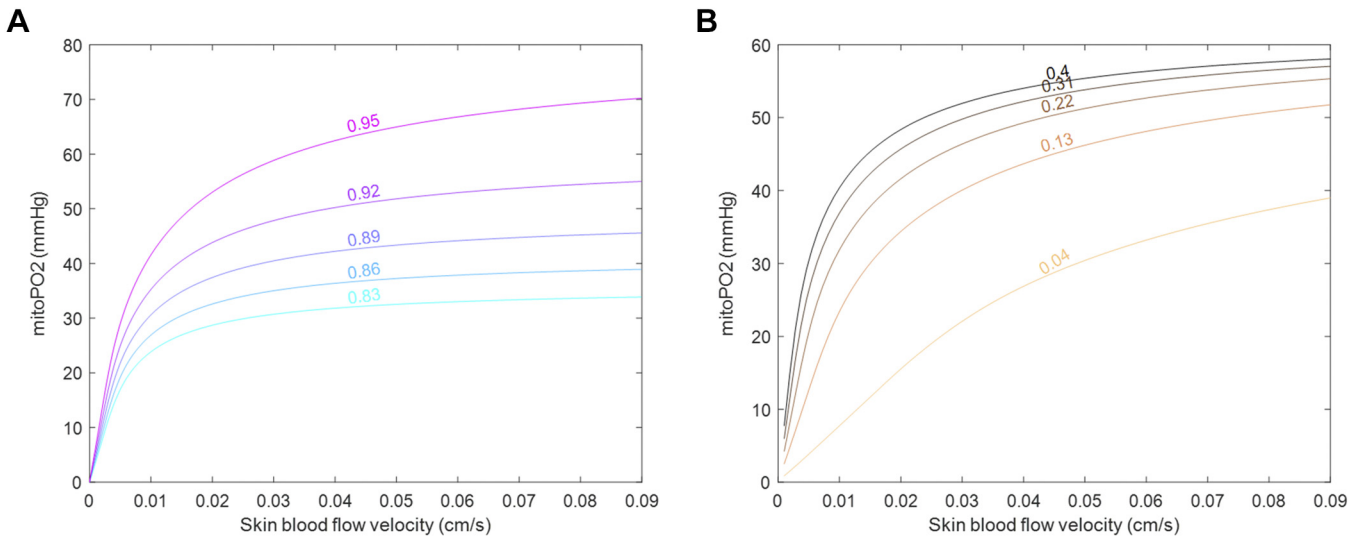


**Figure 4.** Graphs showing relationship of MitoPo$_2$ with skin blood flow velocity for varying $SaO_2$ (*A*) and varying hematocrit (*B*). MitoPo$_2$, mitochondrial oxygen tension in the skin.

resulted in a 5% decrease in mitoPo$_2$ for the complete simulated range of SkBV (Fig. 5*C*).

### The Combined Response of mitoPo$_2$ to Changes in SkBV and Flow Heterogeneity

Figure 6*A* shows a heatmap of the relation between SkBV of the complete microvessel network and the heterogeneity of flow, expressed as the standard deviation of the gamma distribution. Each isoline represents a mitoPo$_2$ step of 3 mmHg. At high SkBV, the effect of heterogeneity (i.e., obstructed flow in capillaries) was relatively small: at flows between 0.06 and 0.09 cm/s, 5 isolines are traversed when moving to maximum flow heterogeneity. In comparison, at intermediate SkBV (0.03–0.06 cm/s), 8–14 isolines are crossed. In addition, at high flow heterogeneity, the relationship of mitoPo$_2$ and SkBV was approximately linear (equal spacing between isolines), whereas at minimal flow heterogeneity, the relationship was exponential (the spaces between isolines increases at higher blood flow velocity). Thus, during severe flow heterogeneity such as in sepsis, to maintain a mitoPo$_2$ of 60 mmHg, SkBV must increase disproportionally high compared with flow heterogeneity.

Figure 6*B* shows the interplay between heterogeneity and mean velocity in the context of shock. A decrease in SkBV from 0.05 cm/s to 0.02 cm/s and concomitant increase in heterogeneity to 0.09 cm/s resulted in a mitoPo$_2$ decrease from 50 mmHg to 5–10 mmHg. Successful resuscitation of flow would result in partial restoration of mitoPo$_2$ (up to 25 mmHg, vertical arrow). Resolving microcirculatory heterogeneity, even without rescued SkBV, resulted in a near complete restoration of mitoPo$_2$ (43 mmHg, horizontal arrow).

We also computed a sensitivity analysis for the variables mentioned previously. The sensitivities are calculated from a range of −25% and 25% of the baseline values of the variables at each 10% interval of SkBV. The numerical sensitivities of the above figures are shown in a heatmap in Fig. 7 and corroborate the graphical results.

### The Combined Response of mitoPo$_2$ to Changes in Oxygen Saturation and SkBV

The response of mitoPo$_2$ to a decrease in saturation is complex (Fig. 8). A normal SkBV of greater than 0.04 cm/s had a protective effect on mitoPo$_2$ during hypoxemia.

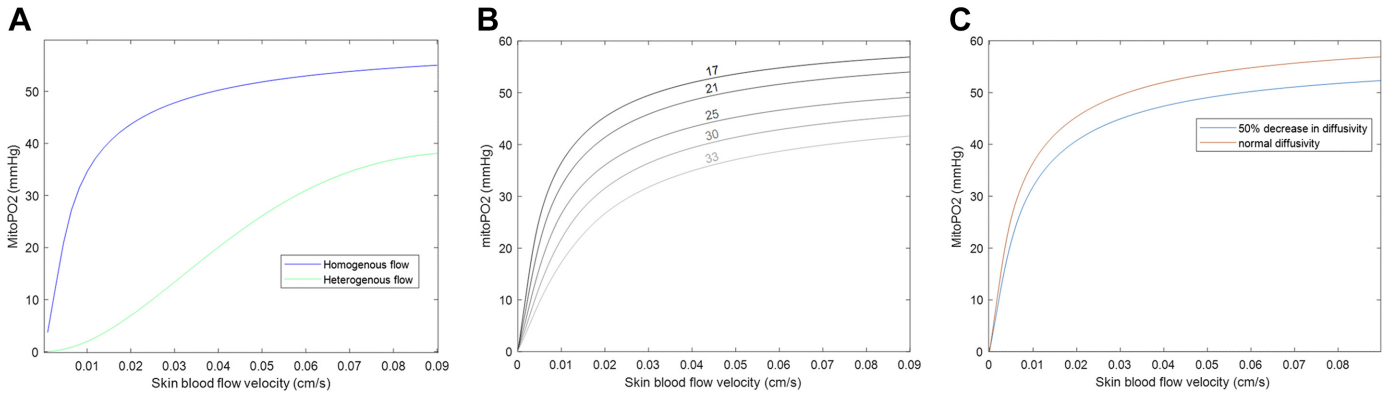


**Figure 5.** Graphs showing relationship of MitoPo$_2$ with SkBV and variation with microcirculatory parameters. *A*: effect of heterogeneous flow on MitoPo$_2$ (blue line, gamma distribution with SD 0.09). *B*: effect of capillary density on MitoPo$_2$ (range between 50 μm and 100 μm). *C*: effect of decrease in diffusivity (blue line, 0.5 × diffusivity) compared with normal (orange line). MitoPo$_2$, mitochondrial oxygen tension in the skin; SkBV, skin blood flow velocity.

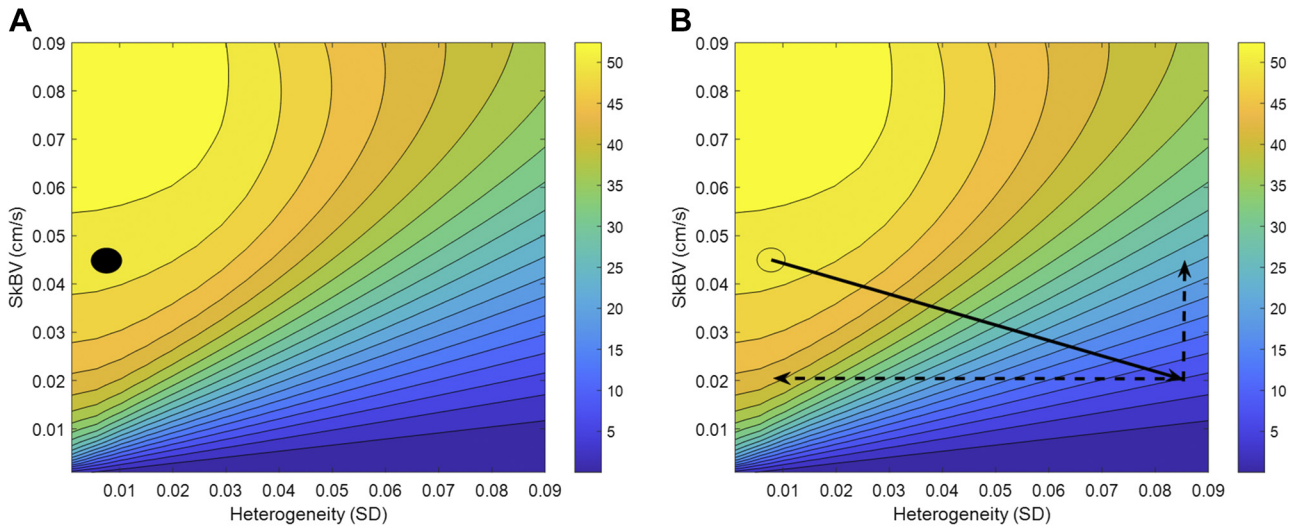


**Figure 6.** *A*: colored heatmap showing MitoPo$_2$ (color from 0 to 70 mmHg) as a function of SkBV and flow heterogeneity. Black dot indicating the normal situation (mean SkBV between 0.04 and 0.05) and minimal flow heterogeneity (SD of 0.01 cm/s) for a MitoPo$_2$ of 60 mmHg. *B*: colored heatmap of MitoPo$_2$ as a function of flow heterogeneity (the standard deviation of gamma distribution of individual velocities) and SkBV. Black lines are the isolines, indicating constant MitoPo$_2$ along the line. Each isoline corresponds to a MitoPo$_2$ step of 3 mmHg. The solid arrow indicates the combined effect of decrease in SkBV and increase in flow heterogeneity in septic shock. The dashed arrows indicate the separate contribution of SkBV and flow heterogeneity. MitoPo$_2$, mitochondrial oxygen tension in the skin; SkBV, skin blood flow velocity.

MitoPo$_2$ decreased with a decrease in saturation, however, mitoPo$_2$ did not decrease below 30 mmHg, even at a saturation of 85% when SkBV is maintained above 0.01 cm/s.

### Clinical Validation of the Model with Data of Patients with Cardiogenic Shock

The scatterplot of mitoPo$_2$ versus lactate in postoperative cardiac surgical patients with cardiogenic shock shows that below a mitoPo$_2$ of 20 mmHg, lactate starts to increase (Fig. 9). It is well known that at a total body OER ($SaO_2 - SvO_2/SaO_2$) of greater than 0.6, anaerobiosis, as evidenced by arterial lactate levels, occurs. The mathematical model predicts that mitoPo$_2$ of 19 mmHg corresponds to an OER in the skin of 0.6. Concurrently, the scatterplot of mitoPo$_2$ versus lactate in postoperative cardiac surgical patients shows that below a mitoPo$_2$ of 20 mmHg, lactate starts to increase above 2 mmol/L.

## DISCUSSION

Using a modified Krogh model, we were able to demonstrate the relationship of mitoPo$_2$ with determinants of

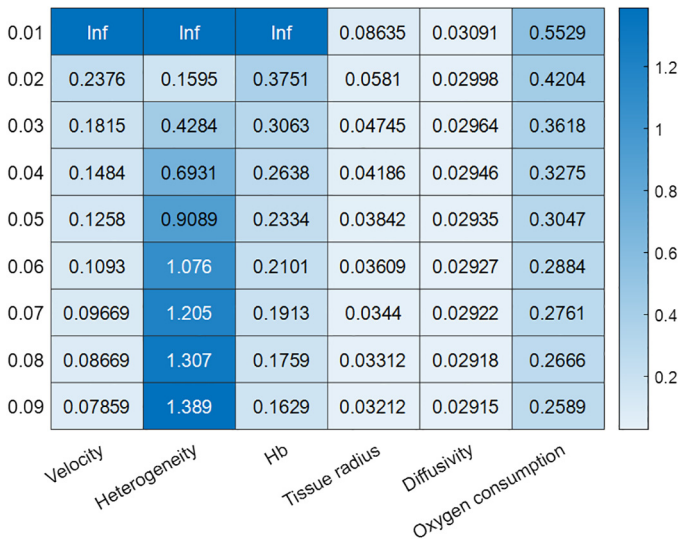


**Figure 7.** Heatmap of sensitivities of main parameters in the model at different values of skin blood flow velocity (*y*-axis). Each SkBV denotes the sensitivity. Sensitivities are computed for ±25% of the range of the baseline values. Darker shades indicate a higher sensitivity. SkBV, skin blood flow velocity.

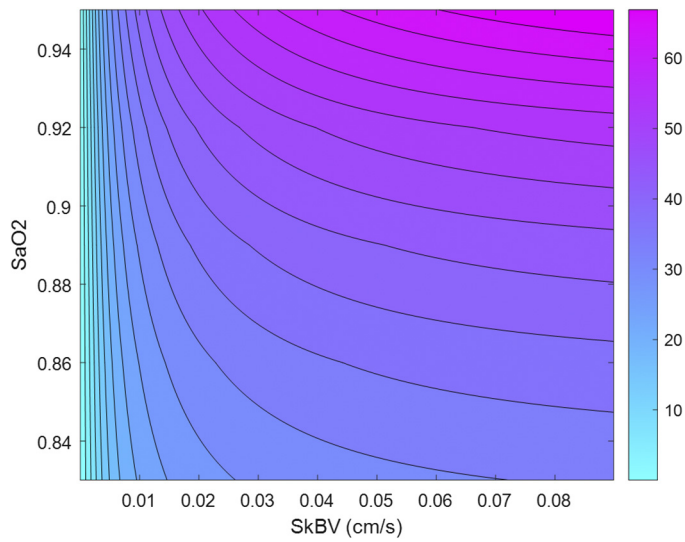


**Figure 8.** Colored heatmap of MitoPo$_2$ as a function of SkBV and Hb $O_2$ saturation (as fraction). Each isoline corresponds to a MitoPo$_2$ step of 6 mmHg. Color indicates MitoPo$_2$ magnitude, ranging from 0 mmHg (blue) to 70 mmHg (purple). MitoPo$_2$, mitochondrial oxygen tension in the skin; SkBV, skin blood flow velocity.

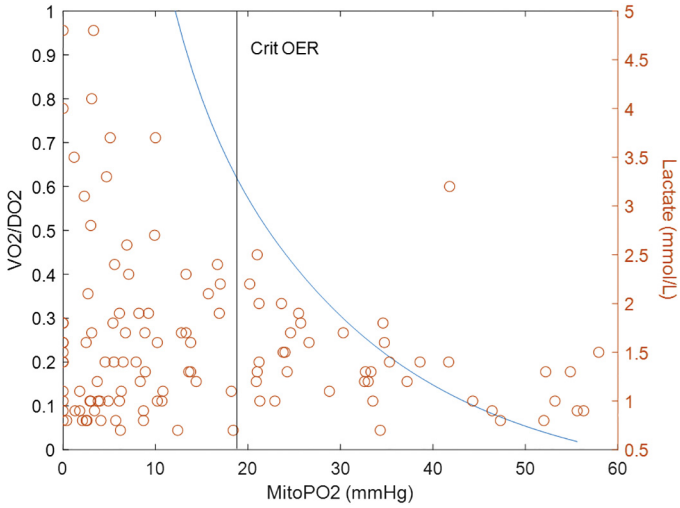


**Figure 9.** MitoPo$_2$ vs. lactate of 44 cardiac surgical patients (orange dots) fitted to the relationship of MitoPo$_2$ with $\dot{V}O_2/DO_2$ (blue) as a proxy of oxygen extraction ratio (OER). The simulation is run with $m$ at $0.35 \times 10^{-4}$ mLO$_2$/mL/s, SaO$_2$ at 92% and a heterogeneity of 0.1 SD. SkBV is varied from 0 cm/s to 0.09 cm/s The line displays the predicted MitoPo$_2$ at local critical OER where anaerobic metabolism occurs. MitoPo$_2$, mitochondrial oxygen tension in the skin; SkBV, skin blood flow velocity.

microcirculatory perfusion. We have demonstrated the validity of the model by fitting the relationship of mitoPo$_2$ with OER to lactate data from patients with cardiogenic shock. Although mathematical simplifications in these relationships should be acknowledged, within these limits, our model infers several properties and characteristics.

### Skin mitoPo$_2$ at Baseline is 40–60 mmHg

The magnitude of the Po$_2$ in mitochondria has been a matter of debate. The conventional view is that Po$_2$ decreases to around 5 mmHg in the mitochondria. This view is based on the oxygen cascade and the often presumed large diffusion distance (57). In contrast, our mathematical simulations for mitochondrial Po$_2$ in skin suggest that mean mitoPo$_2$ is in the range of 40–60 mmHg in physiological steady state (Fig. 3), which approaches intravascular values. In line, mitoPo$_2$ in healthy human volunteers measured with PpIX-TSLT showed values ranging from 50 to 70 mmHg (5, 58–60). Furthermore, studies investigating interstitial tissue Po$_2$ using different techniques have reported similar magnitude of tissue oxygen tension (30–40 mmHg) (61–63). Our model corroborates that if microvascular capillaries are well saturated and have high enough blood flow, the surrounding mean tissue Po$_2$ in skin will reach a similar magnitude. The physiological explanation of a relatively high oxygen tension in the cell is that cellular membranes are not very resistant to oxygen diffusion and thus it is possible for cells close to the arteriolar end to have similar oxygen tension as intravascular tensions (36, 64). In line, even a 50% increase in resistance to oxygen diffusion in our model results in the same magnitude of mitoPo$_2$ (Fig. 5*A*). Our results cannot be extrapolated to mitochondrial oxygen tension in other (vital) organs, as the architecture of the microvasculature, blood flow velocity, and the oxygen consumption can be vastly different from those in the skin.

We have shown that skin mitoPo$_2$ is two orders of magnitude higher than the minimum Po$_2$ required to generate adenosine triphosphate (0.7 mmHg). This does not disprove the possibility of tissue hypoxia in circulatory shock. MitoPo$_2$ is a representation of the average oxygen tension around a network of microvessel and accordingly, hypoxic zones can exist around one microvessel, as first shown by Krogh. The fitting of lactate data of patients with cardiogenic shock to the predicted mitoPo$_2$ at critical global OER shows that the prediction closely follows clinical observations in patients and that a relatively low mitoPo$_2$ (20 mmHg) corresponds to anaerobic metabolism in the model and cardiogenic shock. In addition, previous simulation studies found that at a mean tissue oxygen tension of 30 mmHg, 10% of the tissue surrounding the capillaries was hypoxic (38).

### Skin mitoPo$_2$ Has Threshold Behavior in Response to Decreases in Skin Perfusion and Anemia

The logarithmic shape of the curve in Fig. 3 would render mitoPo$_2$ a threshold marker of shock. Small reductions in SkBV will result in negligible decreases in mitoPo$_2$. However, in response to low cardiac output, SkBV can reach values as low as 0.004 cm/s (65). Thus, as SkBV reaches the critical point of inflection (a SkBV of 0.01 cm/s), mitoPo$_2$ sharply decreases to a mitoPo$_2$ of 10–20 mmHg and thus shows an apparent "skipping" of a range of values. Our simulations show that this behavior also applies to hematocrit. This would imply that mitoPo$_2$ could be a very sensitive marker of reduced peripheral perfusion.

This property of mitoPo$_2$ is also supported by experimental observations. In a pig hemodilution model, mitoPo$_2$ values remained relatively constant with reductions in hematocrit and oxygen delivery but decreased abruptly at a critical point (6). This abrupt decrease occurred when hematocrit decreased from 0.11 to 0.08. In our mathematical simulation, the absolute value of the critical point lies around 0.14. This difference is likely due to interspecies variation; pigs are relatively more anemic, have different skin oxygen consumption, and have a substantially different baseline mitoPo$_2$ compared with humans (20–40 mmHg). The threshold property of SkBV on tissue oxygenation was also illustrated using laser Doppler in critically ill patients treated with 500 mL of fluid removal by dialysis. Large changes in SkBV had very good accuracy in diagnosing tissue hypoxia as measured with lactate, but small changes had low accuracy (66).

### A High Skin Perfusion Protects mitoPo$_2$ from Mild Arterial Hypoxemia

Increasing SkBV made mitoPo$_2$ more sensitive to changes in SaO$_2$. The mathematical and physiological interpretation is that when blood travels very fast along a microvessel, the convective flux of oxygen is maximal. Thus, this flux can only be increased by increasing the oxygen content and the complete tissue radius can reach equilibrium with the partial pressure inside the vessel. Thus, when this partial pressure of oxygen was increased through increasing saturation, the equilibrium between microvessel pressure and tissue pressure (and hence mitoPo$_2$) was at a much higher level. In line with this, studies found that in regions of the brain where cerebral blood flow was compromised, increasing Pa$_{O_2}$ had

little effect on mean tissue oxygen tension but did cause an increase in healthy brain tissue where blood flow was maintained (11, 67–69).

However, it remains to be seen whether this relationship holds true for the internal organs, which autoregulate their blood flow in response to changes in arterial oxygen partial pressure. This is in contrast to the skin, which exhibits little vasoconstriction in response to hyperoxemia (70, 71). There is experimental evidence that hyperoxia dose-dependently increases mito$P_{O_2}$ of the heart and liver until an $F_{I_{O_2}}$ of 40%, after which a plateau is reached (72). However, interpretation of these results is limited by the absence of corresponding Hb-$O_2$ saturation data. The attenuated effect could be the result of compensatory hyperoxic vasoconstriction or more simply, a complete saturation of Hb at $F_{I_{O_2}}$ of 40%. Hence, further studies should be done to assess the interorgan variability of mito$P_{O_2}$ in hyperoxia.

### Microvessel Flow Heterogeneity is a More Important Determinant of Skin mito$P_{O_2}$ than Mean Microvessel Blood Flow

Our mathematical model confirms that of all the microcirculatory disturbances, flow heterogeneity has the most impact on mito$P_{O_2}$ (Fig. 7), in line with previous clinical and modeling studies (13, 15, 29, 47, 56, 73, 74).

Our results show that despite a hyperdynamic cardiac output and blood flow, shock can lead to substantial decrease in mito$P_{O_2}$ through flow heterogeneity. An extremely heterogeneous distribution of flow in the microvessels cannot achieve a high mito$P_{O_2}$, even at supranormal blood flow velocity. This would imply that interventions aimed at "homogenizing" SkBV would restore mito$P_{O_2}$ to a greater effect than increasing mean skin blood flow through an increase in cardiac output, as suggested before (75–77). Whether vasodilating agents can have this effect remains to be determined. Since the first experimental in vivo studies showing the effects of blood flow heterogeneity on tissue oxygenation through advanced NADH video-fluorometry (75, 76), numerous studies have corroborated the importance of heterogeneous flow on tissue oxygen extraction and clinical outcome and subsequent pathogenesis of multiorgan failure in circulatory shock (78). Our results support that theoretically, mito$P_{O_2}$ would be sensitive to detect the changes in microcirculatory integrity.

### Limitations of Our Model

We have evaluated the applicability of mito$P_{O_2}$ in shock and introduced a conceptual framework that follows from the mathematical model. The simulations are made under a myriad of assumptions that can limit the accuracy of the model.

First, we used a combined arteriolar and capillary microvessel with averaged microvessel radius. It is beyond the scope of this paper to model these two as separate compartments with complex anastomoses, and because the basis of most oxygen transport simulation studies has been the Krogh model of a single capillary, we modified it to account for linear arteriolar diffusion as multiple experiments on single red blood cells and capillaries showed that oxygen diffusion occurs at the arteriolar level (25). The experimentally observed oxygen dissipation from arterioles is also shown to be mostly due to the consumption by surrounding parenchyma (24). As mito$P_{O_2}$ can be measured on the complete area of the skin that is saturated with 5-aminolevulinic acid, the tissue-vessel exchange compartment can be considered as one unit, irrespective of the nature of the vessel its effect is small on the average $P_{O_2}$ in tissue.

Second, the model assumes that capillaries are geometrically evenly distributed in the skin with one capillary providing oxygen for a tissue cylinder that is four times its own radius. However, studies have shown that intercapillary distance is highly variable and has a significant effect on tissue $P_{O_2}$ distributions (79, 80). Mito$P_{O_2}$ for these saturations might therefore deviate from experimentally found values. We also did not take into account changes in pH and subsequent effects on Hb-$O_2$ dissociation through changing p50 and Hill constants. Patients in circulatory shock often have derangements in acid-base status and our results are therefore not applicable to patients with severely deranged pH.

In addition, the applicability of this framework in shock is based on the presumption that more intracellular oxygen is "better," however, high partial pressure of oxygen could induce significant vasoconstriction, potentially rendering our equations untrue for high partial pressures of oxygen. Also, high $Pa_{O_2}$ could result in increased production of radical oxygen species, which could damage mitochondria and impair their function. It remains to be investigated to what extent this occurs and whether this is detrimental for tissue viability, offsetting the positive effects of adequate oxygenation of tissues.

Furthermore, the suitability of skin mito$P_{O_2}$ as a marker of shock depends on the flow sensitivity of the cutaneous vasculature. Factors that interfere in the direct coupling between cutaneous vasoconstriction and decreased cardiac output will cause skin mito$P_{O_2}$ to be falsely low. Such factors are (central) hypothermia and peripheral arterial disease. The extent to which this affects mito$P_{O_2}$ should be a focus of further studies.

### Conclusions

Our mathematical model of skin mitochondrial oxygen tension based on Krogh's cylinder model shows that physiological mito$P_{O_2}$ in skin is 40–60 mmHg. The relationship of mito$P_{O_2}$ with skin blood flow velocity follows a logarithmic growth curve, with a critical inflection point at which mito$P_{O_2}$ rapidly deteriorates if peripheral perfusion further decreases. Adequate blood flow is critical to maintain mito$P_{O_2}$ levels, and heterogeneity importantly decreases mito$P_{O_2}$. This mathematical framework may serve to interpret mito$P_{O_2}$ values in shock, with the potential to enhance personalized clinical trial design.

## DATA AVAILABILITY

Data will be made available upon reasonable request.

## GRANTS

Dr. Pillay is supported by the ESICM NEXT startup grant.

## DISCLOSURES

E.G.M. is listed as inventor on patents related to mitochondrial oxygen measurements held by the Academic Medical Center Amsterdam and the Erasmus Medical Center Rotterdam, The Netherlands. E.G.M. is founder and shareholder of Photonics Healthcare, a company that holds exclusive licenses to these patents and that markets the COMET system. None of the other authors has any conflicts of interest, financial or otherwise, to disclose.

## AUTHOR CONTRIBUTIONS

B.N.H. conceived and designed research; B.N.H. performed experiments; B.N.H. analyzed data; B.N.H. and N.P.J. interpreted results of experiments; B.N.H. prepared figures; B.N.H. drafted manuscript; B.N.H., R.F.C., M.B., S.N.A., B.v.d.B., E.G.M., C.I., J.P., and N.P.J. edited and revised manuscript; B.N.H., R.F.C., M.B., S.N.A., B.v.d.B., E.G.M., C.I., J.P., and N.P.J. approved final version of manuscript.

## REFERENCES


1. **Dünser MW**, **Takala J**, **Brunauer A**, **Bakker J.** Re-thinking resuscitation: leaving blood pressure cosmetics behind and moving forward to permissive hypotension and a tissue perfusion-based approach. *Crit Care* 17: 326, 2013. doi:10.1186/cc12727.
2. **Boyd JH**, **Forbes J**, **Nakada T-A**, **Walley KR**, **Russell JA.** Fluid resuscitation in septic shock: a positive fluid balance and elevated central venous pressure are associated with increased mortality. *Crit Care Med* 39: 259–265, 2011. doi:10.1097/CCM.0b013e3181feeb15.
3. **Vallet B**, **Tavernier B**, **Lund N.** Assessment of tissue oxygenation in the critically-ill. *Eur J Anaesthesiol* 17: 221–229, 2000. doi:10.1046/j.1365-2346.2000.00667.x.
4. **Ubbink R**, **Bettink MAW**, **Janse R**, **Harms FA**, **Johannes T**, **Münker FM**, **Mik EG.** A monitor for Cellular Oxygen METabolism (COMET): monitoring tissue oxygenation at the mitochondrial level. *J Clin Monit Comput* 31: 1143–1150, 2017. doi:10.1007/s10877-016-9966-x.
5. **Ubbink R**, **Wefers Bettink MA**, **van Weteringen W**, **Mik EG.** Mitochondrial oxygen monitoring with COMET: verification of calibration in man and comparison with vascular occlusion tests in healthy volunteers. *J Clin Monit Comput* 35: 1357–1366, 2020. doi:10.1007/s10877-020-00602-y.
6. **Römers LHL**, **Bakker C**, **Dollée N**, **Hoeks SE**, **Lima A**, **Raat NJH**, **Johannes T**, **Stolker RJ**, **Mik EG.** Cutaneous mitochondrial Po2, but not tissue oxygen saturation, is an early indicator of the physiologic limit of hemodilution in the pig. *Anesthesiology* 125: 124–132, 2016. doi:10.1097/ALN.0000000000001156.
7. **Wefers Bettink MA**, **Harms FA**, **Dollee N**, **Specht PAC**, **Raat NJH**, **Schoonderwoerd GC**, **Mik EG.** Non-invasive versus ex vivo measurement of mitochondrial function in an endotoxemia model in rat: toward monitoring of mitochondrial therapy. *Mitochondrion* 50: 149–157, 2020. doi:10.1016/j.mito.2019.11.003.
8. **Mik EG**, **Balestra GM**, **Harms FA.** Monitoring mitochondrial Po$_2$: the next step. *Curr Opin Crit Care* 26: 289–295, 2020. doi:10.1097/MCC.0000000000000719.
9. **Goldman D.** Theoretical models of microvascular oxygen transport to tissue. *Microcirculation* 15: 795–811, 2008. doi:10.1080/10739680801938289.
10. **Jung A**, **Faltermeier R**, **Rothoerl R**, **Brawanski A.** A mathematical model of cerebral circulation and oxygen supply. *J Math Biol* 51: 491–507, 2005. doi:10.1007/s00285-005-0343-5.
11. **Sarrafzadeh AS**, **Kiening KL**, **Bardt TF**, **Schneider GH**, **Unterberg AW**, **Lanksch WR.** Cerebral oxygenation in contusioned vs. nonlesioned brain tissue: monitoring of PtiO2 with Licox and Paratrend. *Acta Neurochir Suppl* 71: 186–189, 1998. doi:10.1007/978-3-7091-6475-4_54.
12. **Pittman RN.** Regulation of tissue oxygenation (2nd ed.). *Colloquium Integrated Systems Physiology: From Molecule to Function to Disease*. San Rafael, CA: Morgan & Claypool, 2016.
13. **Østergaard L.** Blood flow, capillary transit times, and tissue oxygenation: the centennial of capillary recruitment. *J Appl Physiol (1985)* 129: 1413–1421, 2020. doi:10.1152/JAPPLPHYSIOL.00537.2020.
14. **Harms FA**, **Ubbink R**, **de Wijs CJ**, **Ligtenberg MP**, **ter Horst M**, **Mik EG.** Mitochondrial oxygenation during cardiopulmonary bypass: a pilot study. *Front Med (Lausanne)* 9: 785734, 2022. doi:10.3389/fmed.2022.785734.
15. **Lücker A**, **Secomb TW**, **Weber B**, **Jenny P.** The relative influence of hematocrit and red blood cell velocity on oxygen transport from capillaries to tissue. *Microcirculation* 24: e12337, 2017. doi:10.1111/micc.12337.
16. **Popel AS**, **Gross JF.** Analysis of oxygen diffusion from arteriolar networks. *Am J Physiol Heart Circ Physiol* 6: H681–H689, 1979. doi:10.1152/ajpheart.1979.237.6.h681.
17. **Vadapalli A**, **Pittman RN**, **Popel AAS.** Estimating oxygen transport resistance of the microvascular wall. *Am J Physiol Heart Circ Physiol* 279: H657–H671, 2000. doi:10.1152/ajpheart.2000.279.2.h657.
18. **Výbohová D**, **Mellová Y**, **Adamicová K**, **Adamkov M**, **Hešková G.** Quantitative changes of the capillary bed in aging human skin. *Histol Histopathol* 27: 961–967, 2012. doi:10.14670/HH-27.961.
19. **Braverman IM.** The cutaneous microcirculation: ultrastructure and microanatomical organization. *Microcirculation* 4: 329–340, 1997. doi:10.3109/10739689709146797.
20. **Schumacker PT**, **Samsel RW.** Analysis of oxygen delivery and uptake relationships in the Krogh tissue model. *J Appl Physiol (1985)* 67: 1234–1244, 1989. doi:10.1152/jappl.1989.67.3.1234.
21. **Favaron E**, **Ince C**, **Hilty MP**, **Ergin B**, **van der Zee P**, **Uz Z**, **Wendel Garcia PD**, **Hofmaenner DA**, **Acevedo CT**, **van Boven WJ**, **Akin S**, **Gommers D**, **Endeman H.** Capillary leukocytes, microaggregates, and the response to hypoxemia in the microcirculation of coronavirus disease 2019 Patients. *Crit Care Med* 49: 661–670, 2021. doi:10.1097/CCM.0000000000004862.
22. **Boerma EC**, **Ince C.** The role of vasoactive agents in the resuscitation of microvascular perfusion and tissue oxygenation in critically ill patients. *Intensive Care Med* 36: 2004–2018, 2010. doi:10.1007/s00134-010-1970-x.
23. **Desjardins C**, **Duling BR.** Microvessel hematocrit: measurement and implications for capillary oxygen transport. *Am J Physiol Heart Circ Physiol* 252: H494–H503, 1987. doi:10.1152/ajpheart.1987.252.3.h494.
24. **Tsai AG**, **Cabrales P**, **Hangai-Hoger N**, **Intaglietta M.** Oxygen distribution and respiration by the microcirculation. *Antioxid Redox Signal* 6: 1011–1018, 2004. doi:10.1089/ars.2004.6.1011.
25. **Tsai AG**, **Johnson PC**, **Intaglietta M.** Oxygen gradients in the microcirculation. *Physiol Rev* 83: 933–963, 2003. doi:10.1152/physrev.00034.2002.
26. **Akons K**, **Dann EJ**, **Yelin D.** Measuring blood oxygen saturation along a capillary vessel in human. *Biomed Opt Express* 8: 5342–5348, 2017. doi:10.1364/boe.8.005342.
27. **Jaszczak P**, **Sejrsen P**, **Sørensen PR.** The influence of the epidermal membrane on percutaneous Po$_2$ and metabolic rate. *Scand J Clin Lab Invest* 48: 17–20, 1988. doi:10.1080/00365518809168182.
28. **Stucker M**, **Baier V**, **Reuther T**, **Hoffman K**, **Kellam K**, **Altmeyer P.** Capillary blood cell velocity in human skin capillaries located perpendicularly to the skin surface. *Microvasc Res* 52: 188–192, 1996. doi:10.1006/mvre.1996.0054.
29. **Edul VSK**, **Enrico C**, **Laviolle B**, **Vazquez AR**, **Ince C**, **Dubin A.** Quantitative assessment of the microcirculation in healthy volunteers and in patients with septic shock. *Crit Care Med* 40: 1443–1448, 2012. doi:10.1097/CCM.0b013e31823dae59.
30. **Grossmann U.** Simulation of combined transfer of oxygen and heat through the skin using a capillary-loop model. *Math Biosci* 61: 205–236, 1982. doi:10.1016/0025-5564(82)90004-9.
31. **McGuire BJ**, **Secomb TW.** A theoretical model for oxygen transport in skeletal muscle under conditions of high oxygen demand. *J Appl Physiol* 91: 2255–2265, 2001. doi:10.1152/jappl.2001.91.5.2255.
32. **Dermol-Černe J**, **Miklavčič D.** From cell to tissue properties-modeling skin electroporation with pore and local transport region formation. *IEEE Trans Biomed Eng* 65: 458–468, 2018. doi:10.1109/TBME.2017.2773126.
33. **Huclova S**, **Erni D**, **Fröhlich J.** Modelling and validation of dielectric properties of human skin in the MHz region focusing on skin layer morphology and material composition. *J Phys D Appl Phys* 45: 025301, 2012. doi:10.1088/0022-3727/45/2/025301.

35. **Schumacker PT**, **Cain SM.** The concept of a critical oxygen delivery. *Intensive Care Med* 13: 223–229, 1987. doi:10.1007/BF00265110.
36. **Popel AS.** Theory of oxygen transport to tissue. *Crit Rev Biomed Eng* 17: 257–321, 1989.
37. **Tenney SM.** A theoretical analysis of the relationship between venous blood and mean tissue oxygen pressures. *Respir Physiol* 20: 283–296, 1974. doi:10.1016/0034-5687(74)90025-5.
38. **Kreuzer F.** Oxygen supply to tissues: the Krogh model and its assumptions. *Experientia* 38: 1415–1426, 1982. doi:10.1007/BF01955753.
39. **Krogh A.** The number and distribution of capillaries in muscles with calculations of the oxygen pressure head necessary for supplying the tissue. *J Physiol* 52: 409–415, 1919. doi:10.1113/jphysiol.1919.sp001839.
40. **Tai RC**, **Chang HK.** Oxygen transport in heterogeneous tissue. *J Theor Biol* 43: 265–276, 1974. doi:10.1016/S0022-5193(74)80059-7.
41. **Venkataraman K**, **Wang T**, **Stroeve P.** Oxygen diffusion into heterogeneous tissue with combined oxygen. *Ann Biomed Eng* 8: 17–27, 1980. doi:10.1007/BF02363168.
42. **Stroeve P.** Diffusion with irreversible chemical reaction in heterogeneous media: application to oxygen transport in respiring tissue. *J Theor Biol* 64: 237–251, 1977. doi:10.1016/0022-5193(77)90354-X.
43. **Clark A**, **Clark PA**, **Connett RJ**, **Gayeski TE**, **Honig CR.** How large is the drop in P($O_2$) between cytosol and mitochondrion? *Am J Physiol Cell Physiol* 252: C583–C587, 1987. doi:10.1152/ajpcell.1987.252.6.c583.
44. **Clark A Jr**, **Clark PA.** Local oxygen gradients near isolated mitochondria. *Biophys J* 48: 931–938, 1985. doi:10.1016/S0006-3495(85)83856-X.
45. **Mainwood GW**, **Rakusan K.** A model for intracellular energy transport. *Can J Physiol Pharmacol* 60: 98–102, 1982. doi:10.1139/y82-016.
46. **Popel AS.** Theory of oxygen transport to tissue. *Crit Rev Biomed Eng* 17: 139–148, 2017.
47. **Jespersen SN**, **Østergaard L.** The roles of cerebral blood flow, capillary transit time heterogeneity, and oxygen tension in brain oxygenation and metabolism. *J Cereb Blood Flow Metab* 32: 264–277, 2012. doi:10.1038/jcbfm.2011.153.
48. **Grinberg O**, **Novozhilov B**, **Grinberg S**, **Friedman B**, **Swartz HM.** Axial oxygen diffusion in the Krogh model: modifications to account for myocardial oxygen tension in isolated perfused rat hearts measured by EPR oximetry. *Adv Exp Med Biol* 566: 127–134, 2005. doi:10.1007/0-387-26206-7_18.
49. **Szeimies RM**, **Sassy T**, **Landthaler M.** Penetration potency of topical applied δ-aminolevulinic acid for photodynamic therapy of basal cell carcinoma. *Photochem Photobiol* 59: 73–76, 1994. doi:10.1111/j.1751-1097.1994.tb05003.x.
50. **Cevc G**, **Vierl U.** Spatial distribution of cutaneous microvasculature and local drug clearance after drug application on the skin. *J Control Release* 118: 18–26, 2007. doi:10.1016/j.jconrel.2006.10.022.
51. **Jung F**, **Pindur G**, **Hiebl B**, **Franke RP.** Influence of capillary geometry on hypoperfusion-induced ischemia: a numerical study. *Appl Cardiopulm Pathophysiol* 14: 229–235, 2010.
52. **Mongkolpun W**, **Orbegozo D**, **Cordeiro CPR**, **Franco CJCS**, **Vincent JL**, **Creteur J.** Alterations in skin blood flow at the fingertip are related to mortality in patients with circulatory shock. *Crit Care Med* 48: 443–450, 2020. doi:10.1097/CCM.0000000000004177.
53. **Parpaleix A**, **Houssen YG**, **Charpak S.** Imaging local neuronal activity by monitoring $Po_2$ transients in capillaries. *Nat Med* 19: 241–246, 2013. doi:10.1038/nm.3059.
54. **Hsu R**, **Secomb TW.** Analysis of oxygen exchange between arterioles and surrounding capillary-perfused tissue. *J Biomech Eng* 114: 227–231, 1992. doi:10.1115/1.2891376.
55. **Angleys H**, **Jespersen SN**, **Østergaard L.** The effects of capillary transit time heterogeneity on the BOLD signal. *Hum Brain Mapp* 39: 2329–2352, 2018. doi:10.1002/hbm.23991.
56. **Angleys H**, **Østergaard L.** Krogh's capillary recruitment hypothesis, 100 years on: is the opening of previously closed capillaries necessary to ensure muscle oxygenation during exercise? *Am J Physiol Heart Circ Physiol* 318: H425–H447, 2020. doi:10.1152/ajpheart.00384.2019.
57. **Biro GP.** From the atmosphere to the mitochondrion: the oxygen cascade. In: *Hemoglobin-Based Oxygen Carriers as Red Cell Substitutes and Oxygen Therapeutics*, edited by Kim HW, Greenberg AG. Berlin: Springer, 2013, p. 27–53. doi:10.1007/978-3-642-40717-8_2.
58. **Baumbach P**, **Schmidt-Winter C**, **Hoefer J**, **Derlien S**, **Best N**, **Herbsleb M**, **Coldewey SM.** A pilot study on the association of mitochondrial oxygen metabolism and gas exchange during cardiopulmonary exercise testing: is there a mitochondrial threshold? *Front Med (Lausanne)* 7: 585462, 2020. doi:10.3389/fmed.2020.585462.
59. **Harms FA**, **Voorbeijtel WJ**, **Bodmer SIA**, **Raat NJH**, **Mik EG.** Cutaneous respirometry by dynamic measurement of mitochondrial oxygen tension for monitoring mitochondrial function in vivo. *Mitochondrion* 13: 507–514, 2013. doi:10.1016/j.mito.2012.10.005.
60. **Harms F**, **Stolker RJ**, **Mik E.** Cutaneous respirometry as novel technique to monitor mitochondrial function: a feasibility study in healthy volunteers. *PLoS One* 11: e0159544, 2016. doi:10.1371/journal.pone.0159544.
61. **Vincent JL**, **Moraine JJ**, **van der Linden P.** Toe temperature versus transcutaneous oxygen tension monitoring during acute circulatory failure. *Intensive Care Med* 14: 64–68, 1988. doi:10.1007/BF00254125.
62. **Cody C**, **Buggy DJ**, **Marsh B**, **Moriarity DC.** Subcutaneous tissue oxygen tension after coronary revascularisation with and without cardiopulmonary bypass. *Anaesthesia* 59: 237–242, 2004. doi:10.1111/j.1365-2044.2004.03608.x.
63. **Lübbers DW.** Theory and development of transcutaneous oxygen pressure measurement. *Int Anesthesiol Clin* 25: 31–65, 1987. doi:10.1097/00004311-198702530-00005.
64. **Hellums JD.** The resistance to oxygen transport in the capillaries relative to that in the surrounding tissue. *Microvasc Res* 13: 131–136, 1977. doi:10.1016/0026-2862(77)90122-4.
65. **Wettstein R**, **Tsai AG**, **Erni D**, **Winslow RM**, **Intaglietta M.** Resuscitation with polyethylene glycol-modified human hemoglobin improves microcirculatory blood flow and tissue oxygenation after hemorrhagic shock in awake hamsters. *Crit Care Med* 31: 1824–1830, 2003. doi:10.1097/01.CCM.0000069340.16319.F2.
66. **Mongkolpun W**, **Bakos P**, **Vincent J-L**, **Creteur J.** Monitoring skin blood flow to rapidly identify alterations in tissue perfusion during fluid removal using continuous veno-venous hemofiltration in patients with circulatory shock. *Ann Intensive Care* 11: 59, 2021. doi:10.1186/s13613-021-00847-z.
67. **Hlatky R**, **Valadka AB**, **Gopinath SP**, **Robertson CS.** Brain tissue oxygen tension response to induced hyperoxia reduced in hypoperfused brain. *J Neurosurg* 108: 53–58, 2008. doi:10.3171/JNS/2008/108/01/0053.
68. **Longhi L**, **Valeriani V**, **Rossi S**, **De Marchi M**, **Egidi M**, **Stocchetti N.** Effects of hyperoxia on brain tissue oxygen tension in cerebral focal lesions. *Acta Neurochir Suppl* 81: 315–317, 2002. doi:10.1007/978-3-7091-6738-0_80.
69. **Kiening KL**, **Schneider GH**, **Bardt TF**, **Unterberg AW**, **Lanksch WR.** Bifrontal measurements of brain tissue-$PO_2$ in comatose patients. *Acta Neurochir Suppl* 71: 172–173, 1998. doi:10.1007/978-3-7091-6475-4_50.
70. **Rousseau A**, **Steinwall I**, **Woodson RD**, **Sjöberg F.** Hyperoxia decreases cutaneous blood flow in high-perfusion areas. *Microvasc Res* 74: 15–22, 2007. doi:10.1016/j.mvr.2007.02.001.
71. **Smit B**, **Smulders YM**, **Eringa EC**, **Oudemans-van Straaten H**, **Girbes ARJ**, **Wever KE**, **Hoojimans CR**, **Spoelstra-de Man AME** Effects of hyperoxia on vascular tone in animal models: Systematic review and meta-analysis. *Crit Care* 22: 189, 2018. doi:10.1186/s13054-018-2123-9.
72. **Mik EG**, **Ince C**, **Eerbeek O**, **Heinen A**, **Stap J**, **Hooibrink B**, **Schumacher CA**, **Balestra GM**, **Johannes T**, **Beek JF**, **Nieuwenhuis AF**, **van Horssen P**, **Spaan JA**, **Zuurbier CJ.** Mitochondrial oxygen tension within the heart. *J Mol Cell Cardiol* 46: 943–951, 2009. doi:10.1016/j.yjmcc.2009.02.002.
73. **Ellis CG**, **Wrigley SM**, **Groom AC.** Heterogeneity of red blood cell perfusion in capillary networks supplied by a single arteriole in resting skeletal muscle. *Circ Res* 75: 357–368, 1994. doi:10.1161/01.RES.75.2.357.
74. **Ellis CG**, **Jagger J**, **Sharpe M.** The microcirculation as a functional system. *Crit Care* 9: S3–S8, 2005. doi:10.1186/cc3751.
75. **Ince C**, **Ashruf JF**, **Avontuur JAM**, **Wieringa PA**, **Spaan JAE**, **Bruining HA.** Heterogeneity of the hypoxic state in rat heart is determined at capillary level. *Am J Physiol Heart Circ Physiol* 264: H294–H301, 1993. doi:10.1152/ajpheart.1993.264.2.h294.

76. **Ince C**, **Sinaasappel M.** Microcirculatory oxygenation and shunting in sepsis and shock. *Crit Care Med* 27: 1369–1377, 1999. doi:10.1097/00003246-199907000-00031.
77. **Kara A**, **Akin S**, **Ince C.** Monitoring microcirculation in critical illness. *Curr Opin Crit Care* 22: 444–452, 2016. doi:10.1097/MCC.0000000000000335.
78. **Vincent JL**, **De Backer D.** Microvascular dysfunction as a cause of organ dysfunction in severe sepsis. *Crit Care* 9 *Suppl* 4: S9–S12, 2005. doi:10.1186/cc3748.
79. **Hoofd L**, **Turek Z**, **Kubat K**, **Ringnalda BE**, **Kazda S.** Variability of intercapillary distance estimated on histological sections of rat heart. *Adv Exp Med Biol* 191: 239–247, 1985. doi:10.1007/978-1-4684-3291-6_24.
80. **Kissane RWP**, **Al-Shammari AA**, **Egginton S.** The importance of capillary distribution in supporting muscle function, building on Krogh's seminal ideas. *Comp Biochem Physiol A Mol Integr Physiol* 254: 110889, 2021. doi:10.1016/j.cbpa.2020.110889.